



ERNEST ORLANDO LAWRENCE BERKELEY NATIONAL LABORATORY

Third-Order Semi-Discrete Central Scheme for Conservation Laws and Convection-Diffusion Equations

Alexander Kurganov and Doron Levy

Computing Sciences Directorate
Mathematics Department

June 1999

To be submitted
for publication.



REFERENCE COPY |
Does Not |
Circulate |
Bldg. 50 Library - Ref.
Lawrence Berkeley National Laboratory

DISCLAIMER

This document was prepared as an account of work sponsored by the United States Government. While this document is believed to contain correct information, neither the United States Government nor any agency thereof, nor the Regents of the University of California, nor any of their employees, makes any warranty, express or implied, or assumes any legal responsibility for the accuracy, completeness, or usefulness of any information, apparatus, product, or process disclosed, or represents that its use would not infringe privately owned rights. Reference herein to any specific commercial product, process, or service by its trade name, trademark, manufacturer, or otherwise, does not necessarily constitute or imply its endorsement, recommendation, or favoring by the United States Government or any agency thereof, or the Regents of the University of California. The views and opinions of authors expressed herein do not necessarily state or reflect those of the United States Government or any agency thereof or the Regents of the University of California.

**THIRD-ORDER SEMI-DISCRETE CENTRAL SCHEME
FOR CONSERVATION LAWS AND CONVECTION-DIFFUSION EQUATIONS***

Alexander Kurganov
Department of Mathematics
University of Michigan
Ann Arbor, MI 48109

and

Doron Levy
Department of Mathematics
University of California at Berkeley
and
Computing Sciences Directorate
Lawrence Berkeley National Laboratory
Berkeley, CA 94720, USA

June 1999

*This work was supported in part by the Office of Science, Office of Advanced Scientific Computing Research, Mathematical, Information, and Computational Sciences Division, Applied Mathematical Sciences Subprogram, of the U.S. Department of Energy, under Contract No. DE-AC03-76SF00098.

A Third-Order Semi-Discrete Central Scheme for Conservation Laws and Convection-Diffusion Equations

Alexander Kurganov[†]

Doron Levy[‡]

Abstract

We present a new third-order, semi-discrete, central method for approximating solutions to multi-dimensional systems of hyperbolic conservation laws, convection-diffusion equations, and related problems. Our method is a high-order extension of the recently proposed second-order, semi-discrete method in [16].

The method is derived independently of the specific piecewise polynomial reconstruction which is based on the previously computed cell-averages. We demonstrate our results, by focusing on the new third-order CWENO reconstruction presented in [21]. The numerical results we present, show the desired accuracy, high resolution and robustness of our method.

Key words. Hyperbolic systems, convection-diffusion equations, central difference schemes, high-order accuracy, non-oscillatory schemes, WENO reconstruction.

AMS(MOS) subject classification. Primary 65M10; secondary 65M05.

1 Introduction

Numerical methods for approximating solutions of hyperbolic conservation laws,

$$\frac{\partial}{\partial t}u(x, t) + \frac{\partial}{\partial x}f(u(x, t)) = 0, \quad (1.1)$$

and of the related convection-diffusion equations,

$$\frac{\partial}{\partial t}u(x, t) + \frac{\partial}{\partial x}f(u(x, t)) = \frac{\partial}{\partial x}Q[u(x, t), u_x(x, t)], \quad (1.2)$$

have attracted a lot of attention in recent years (see, e.g., [6, 34], and the references therein). Here, $u(x, t)$ is a conserved quantity, $f(u)$ is a nonlinear convection flux and $Q(u, u_x)$ is a

[†]Department of Mathematics, University of Michigan, Ann Arbor, MI 48109; kurganov@math.lsa.umich.edu

[‡]Department of Mathematics, University of California, Berkeley, CA 94720, and Lawrence Berkeley National Lab; dlevy@math.berkeley.edu

dissipation flux satisfying the (weak) parabolicity condition, $\frac{\partial}{\partial s}Q(u, s) \geq 0$, $\forall u, s$. In the most general case $u = (u_1, \dots, u_n)$ is an n -vector in the d -spatial variables, $x = (x_1, \dots, x_d)$, and f and Q are vector-functions.

In this paper, we focus on the class of *central schemes*, all of which can be viewed as an extension of the well-known Lax-Friedrichs (LxF) scheme, [5]. The first-order LxF method enjoys the major advantage of simplicity over the upwind schemes (e.g., the Godunov scheme, [7]): no (approximate) Riemann solvers or characteristic decompositions are involved in its construction, and therefore, its realization for complicated multi-dimensional systems is rather simple. At the same time, the LxF scheme suffers from excessive numerical dissipation, which causes a poor (smeared) resolution of discontinuities and rarefaction waves.

A second-order, non-oscillatory central scheme was first introduced by Nessyahu and Tadmor in [29]. Since then, the Nessyahu-Tadmor (NT) scheme was further extended to higher orders of accuracy, [27] (also see [3, 19]), as well as to the multi-dimensional systems (1.1), in [1] and [12], (also [18, 20, 21, 22]).

The main ingredient in the construction of the NT method is a second-order, non-oscillatory, MUSCL-type [17], piecewise linear interpolant (instead of the piecewise constant one, employed in the LxF scheme) in combination with the exact solver for the time evolution. This approach allows to significantly improve the resolution of non-smooth solutions to hyperbolic conservation laws, (1.1), while retaining the main advantage of the LxF scheme – *simplicity*.

Unfortunately, applying the fully-discrete NT scheme (or its higher-order extensions) to the second-order convection-diffusion equations, (1.2), does not provide the desired resolution of discontinuities (see, e.g., [14, 15, 16]). This loss of resolution occurs due to the accumulation of excessive numerical dissipation, which is typical of fully-discrete central schemes with small time-steps $\Delta t \sim (\Delta x)^2$ (see [16] for details).

To circumvent this difficulty, a second-order *semi-discrete* central scheme was introduced by Kurganov and Tadmor in [16]. This scheme has smaller dissipation than the NT scheme, and unlike the fully-discrete central schemes, it can be efficiently used with time-steps as small as required by the CFL stability restriction.

The basic idea in the construction of the second-order semi-discrete scheme was to use a more accurate information about the *local* speed of propagation of the discontinuities. One was then able to derive a non-staggered semi-discrete central method, by first integrating over non-equally spaced control volumes, out of which a new piecewise linear interpolant was reconstructed and finally projected on its cell-averages (without evolving in time). The final step, was first introduced in [10], in a somewhat different context of transforming staggered methods into non-staggered methods.

In this paper we extend the results of [16] by introducing a new *third-order, semi-discrete, central scheme*. Our new scheme is derived in a general form which is independent of the reconstruction step, as long as the reconstructed interpolant is sufficiently accurate and non-oscillatory. In particular, we use the new third-order CWENO reconstruction proposed in [21]. This reconstruction provides a third-order accurate interpolant which is built from the given cell-averages such that it is non-oscillatory in the essentially non-oscillatory (ENO) sense (see [9], [31]). This interpolant is written as a convex combination of two one-sided linear functions and one centered parabola. In smooth regions this convex combination guarantees the desired third-order accuracy. It automatically switches to a second-order,

one-sided, linear reconstruction in the presence of large gradients. Such weighted essentially non-oscillatory (WENO) reconstructions were first introduced in the upwind framework, [11, 26], after which they were extended to the central framework, [19, 20, 21, 22].

This paper is organized as follows. We start in §2 with a brief overview of central schemes for conservation laws. In particular we focus in §2.1 on the CWENO reconstruction which we use as the building block for our third-order method below.

We then proceed to construct our new third-order scheme. First, we deal with the fully-discrete, one-dimensional setup in §3. This new fully-discrete scheme is sketched in equation (3.7). We only give the required details that are necessary to fulfill our final goal, namely, to derive the semi-discrete scheme.

With the fully-discrete scheme, (3.7), we are ready to approach the semi-discrete limit in §4.1. Our new third-order, one-dimensional, semi-discrete scheme is then summarized in equation (4.4). This scheme is written in a general form which is independent of the reconstruction step and can also be combined with any appropriate ODE solver for carrying out the time evolution. In §4.2 we then extend our semi-discrete scheme to multidimensional hyperbolic and (degenerate) parabolic problems.

We end by presenting several numerical examples in §5, in which we approximate solutions to hyperbolic conservation laws as well as to convection-diffusion equations. Our new method is shown to enjoy the expected high-accuracy as well as the robustness and the simplicity of the entire family of central schemes.

2 Central Schemes for Conservation Laws

We briefly overview the framework of central schemes for conservation laws. Consider the one-dimensional system (1.1). To approximate its solutions, we introduce a spatial scale, Δx , and integrate over the cell $I(x) := \{\xi \mid |\xi - x| \leq \Delta x/2\}$,

$$\bar{u}_t + \frac{1}{\Delta x} \left[f\left(u\left(x + \frac{\Delta x}{2}, t\right)\right) + f\left(u\left(x - \frac{\Delta x}{2}, t\right)\right) \right] = 0. \quad (2.1)$$

Here and below, \bar{u} denotes the average of u over I ,

$$\bar{u}(x, t) := \frac{1}{\Delta x} \int_{I(x)} u(\xi, t) d\xi.$$

Introducing a time scale, Δt , integrating in time from t to $t + \Delta t$ and sampling (2.1) at the cells $[x_j, x_{j+1}]$, we obtain

$$\bar{u}_{j+1/2}^{n+1} = \bar{u}_{j+1/2}^n - \frac{1}{\Delta x} \int_{\tau=t^n}^{t^{n+1}} [f(u(x_{j+1}, \tau)) - f(u(x_j, \tau))] d\tau, \quad (2.2)$$

where $x_j := j\Delta x$, $t^n := n\Delta t$, $u_j^n := u(x_j, t^n)$ and $\bar{u}_j^n := \bar{u}(x_j, t^n)$. Assuming that at time $t = t^n$ we have computed the cell-averages of the approximate solution, $\{\bar{u}_j^n\}$, we would like

to utilize (2.2) to compute the cell-averages at the next time level, $t^{n+1} = t^n + \Delta t$. To that extent, we introduce a piecewise-polynomial reconstruction,

$$u(x, t^n) \approx \sum_j P_j(x) \chi_j(x), \quad (2.3)$$

where $\chi_j(x)$ is the characteristic function of the cell $I_j := I(x_j)$, and $P_j(x)$ is a polynomial which is reconstructed from the computed cell-averages, $\{\bar{u}_j^n\}$. The degree of the polynomial depends on the desired order of accuracy of the method. Having such an approximation to $u(x, t^n)$, (2.3), we can easily compute the RHS of (2.2). The first term, $\bar{u}_{j+1/2}^n$, equals

$$\bar{u}_{j+1/2}^n = \int_{x_j}^{x_{j+1/2}} P_j(x) dx + \int_{x_{j+1/2}}^{x_{j+1}} P_{j+1}(x) dx.$$

For a sufficiently small time-step, Δt , the solution of (1.1) subject to the initial data (2.3), prescribed at time $t = t^n$, will remain smooth at some neighborhood of the grid points x_j for $t \in [t^n, t^{n+1}]$. Hence, the integrals on the RHS of (2.2) can be approximated using a sufficiently accurate quadrature, which is determined by the overall desired accuracy of the method. The values at the intermediate times which will be required in the quadrature, can be predicted either by a Taylor expansion or using a Runge-Kutta method (consult [3, 19, 27, 29]).

For example, a piecewise-constant reconstruction, $P_j(x) = \bar{u}_j^n$, and a first-order quadrature,

$$\int_{t^n}^{t^{n+1}} f(u(t)) dt \sim \Delta t f(\bar{u}^n),$$

will result with the staggered-LxF scheme (with $\lambda := \Delta t / \Delta x$ denoting the mesh ratio),

$$\bar{u}_{j+1/2}^{n+1} = \frac{\bar{u}_{j+1}^n + \bar{u}_j^n}{2} - \lambda (f(\bar{u}_{j+1}^n) - f(\bar{u}_j^n)).$$

A piecewise linear reconstruction, $P_j(x) = \bar{u}_j^n + (u_x)_j^n (x - x_j)$, with a second-order quadrature in time (such as the mid-point rule), results with the Nessyahu-Tadmor (NT) scheme. Applying nonlinear limiters on the discrete slopes, $(u_x)_j^n$, will prevent oscillations (for details, see [29]).

To obtain a third-order central scheme, one should use a third-order, piecewise parabolic reconstruction together with a more accurate quadrature in time, e.g., Simpson's quadrature rule (see [27] for details).

Remarks:

1. **robustness.** In order to reconstruct a non-oscillatory interpolant, one typically is required to use nonlinear limiters. These limiters decrease the order of accuracy of the method at extrema and by that they play a stabilizing role (e.g., see [17, 27, 29, 34]).

2. **numerical dissipation and time step.** When using fully-discrete central schemes to approximate solutions of convection-diffusion equations, (1.2), the stability restriction enforces small time-steps, $\Delta t \sim (\Delta x)^2$. That is why the numerical dissipation is accumulated and we do not obtain high resolution of discontinuities (see [16] for details).

This problem can be avoided by using semi-discrete schemes instead of the fully-discrete schemes. Such a second-order, central, semi-discrete scheme was introduced in [16]. In this paper we develop a third-order, central, semi-discrete scheme with small numerical dissipation, which can be efficiently used with the small time-steps required due to the second-order operators.

3. **upwind schemes.** Sampling (2.1) at the cells I_j , will result with upwind schemes. Here, one remains with the discontinuities along the interfaces and is bound to solve the Riemann problems there, or at least to approximate their solutions. In the scalar, one-dimensional case this can be easily accomplished, but the Riemann problem has no known solution in the general case of systems and/or several space dimensions.

This is the reason for why central schemes can be considered as universal methods for solving hyperbolic conservation laws: Riemann solvers are not involved in their construction, and moreover, since (2.2) can be carried out componentwise, no characteristic decomposition is required.

2.1 CWENO reconstruction

The first one-dimensional, third-order central scheme in [27], implemented the non-oscillatory piecewise parabolic reconstruction proposed by Liu and Osher in [25]. Since then, a variety of simpler reconstructions has appeared in the literature. Among these, we would like to mention the Central-ENO reconstruction in [3] and the Central-WENO (CWENO) reconstruction in [19] and [21], which was extended to the two-dimensional setup in [20] and [22].

Our new third-order semi-discrete method which we develop in §3 and §4 below, can be integrated with any third-order, non-oscillatory reconstruction. In our numerical simulations presented in §5, we will use the method recently presented in [21], which we will now briefly overview.

In each cell I_j we reconstruct a quadratic polynomial as a convex combination of three polynomials $P_L(x)$, $P_R(x)$ and $P_C(x)$,

$$P_j(x) = w_L P_L(x) + w_R P_R(x) + w_C P_C(x), \quad (2.4)$$

with positive weights $w_i \geq 0$, $\forall i \in \{c, r, l\}$, and $\sum_i w_i = 1$. The polynomials $P_L(x)$, $P_R(x)$ correspond to left and right one-sided linear reconstructions, respectively, while $P_C(x)$ is a parabola, centered around x_j .

The linear functions, $P_R(x)$ and $P_L(x)$, are uniquely determined by requiring them to conserve the one-sided cell averages (\bar{u}_j^n , \bar{u}_{j+1}^n and \bar{u}_j^n , \bar{u}_{j-1}^n , respectively) as

$$P_R(x) = \bar{u}_j^n + \frac{\bar{u}_{j+1}^n - \bar{u}_j^n}{\Delta x}(x - x_j), \quad P_L(x) = \bar{u}_j^n + \frac{\bar{u}_j^n - \bar{u}_{j-1}^n}{\Delta x}(x - x_j). \quad (2.5)$$

The centered parabola, $P_C(x)$, is chosen such as to satisfy,

$$P_{\text{EXACT}}(x) = c_L P_L(x) + c_R P_R(x) + (1 - c_L - c_R) P_C(x), \quad (2.6)$$

with constants c_i 's. Here, $P_{\text{EXACT}}(x)$ is the unique parabola that conserves the three cell averages, \bar{u}_{j-1}^n , \bar{u}_j^n and \bar{u}_{j+1}^n , which is given by

$$P_{\text{EXACT}}(x) = u_j^n + u_j'(x - x_j) + \frac{1}{2} u_j''(x - x_j)^2. \quad (2.7)$$

The approximations to the point-values of $u(x_j, t^n)$, $u_x(x_j, t^n)$ and $u_{xx}(x_j, t^n)$, are denoted by u_j^n , u_j' , u_j'' and are given by

$$\begin{aligned} u_j^n &= \bar{u}_j^n - \frac{1}{24}(\bar{u}_{j+1}^n - 2\bar{u}_j^n + \bar{u}_{j-1}^n), \\ u_j' &= \frac{\bar{u}_{j+1}^n - \bar{u}_{j-1}^n}{2\Delta x}, \quad u_j'' = \frac{\bar{u}_{j-1}^n - 2\bar{u}_j^n + \bar{u}_{j+1}^n}{\Delta x^2} \end{aligned}$$

In [21] it was shown that every symmetric selection of the constants c_i 's in (2.6) will provide the desired third-order accuracy. For example, by taking, $c_L = c_R = 1/4$, equations (2.5)–(2.7) yield

$$\begin{aligned} P_C(x) &= \bar{u}_j^n - \frac{1}{12}(\bar{u}_{j+1}^n - 2\bar{u}_j^n + \bar{u}_{j-1}^n) + \\ &+ \frac{\bar{u}_{j+1}^n - \bar{u}_{j-1}^n}{2\Delta x}(x - x_j) + \frac{\bar{u}_{j-1}^n - 2\bar{u}_j^n + \bar{u}_{j+1}^n}{\Delta x^2}(x - x_j)^2. \end{aligned} \quad (2.8)$$

In smooth regions, the coefficients w_i of the convex combination in (2.4) are chosen to guarantee the maximum order of accuracy (in this particular case – order three), but in the presence of a discontinuity they are automatically switched to the best one-sided stencil (which generates the least oscillatory reconstruction). The weights are taken as

$$w_i = \frac{\alpha_i}{\sum_i \alpha_i}, \quad \text{where} \quad \alpha_i = \frac{c_i}{(\epsilon + IS_i)^p}, \quad i \in \{C, R, L\}. \quad (2.9)$$

The constant ϵ guarantees that the denominator does not vanish and is taken as $\epsilon = 10^{-6}$. The value of p may be chosen to provide the highest accuracy in smooth areas and ensure the non-oscillatory nature of the solution near the discontinuities (consult [11], see also [19, 21]). In [11] the value $p = 2$ was empirically selected, and here we use the same p in most of the examples presented below. Finally, the smoothness indicators, IS_i , are defined as

$$IS_i = \sum_{l=1}^2 \int_{x_{j-1/2}}^{x_{j+1/2}} (\Delta x)^{2l-1} (P_i^{(l)}(x))^2 dx.$$

A direct computation then results with

$$\begin{aligned} IS_L &= (\bar{u}_j^n - \bar{u}_{j-1}^n)^2, \quad IS_R = (\bar{u}_{j+1}^n - \bar{u}_j^n)^2, \\ IS_C &= \frac{13}{3}(\bar{u}_{j+1}^n - 2\bar{u}_j^n + \bar{u}_{j-1}^n)^2 + \frac{1}{4}(\bar{u}_{j+1}^n - \bar{u}_{j-1}^n)^2. \end{aligned} \quad (2.10)$$

It is easy to see that in the presence of large gradients, this reconstruction switches to one of the second-order one-sided linear reconstructions, P_R or P_L . For more details we refer to [21].

3 The Fully-Discrete One-Dimensional Construction

In this section we present the new third-order method in the fully-discrete framework. Since we are mainly interested in deriving the semi-discrete scheme, we will concentrate only on the details which are required for that task. The scheme we derive here, is a third-order extension of the fully-discrete second-order scheme presented in [16].

Following [16], we would like to augment the integration over the Riemann fans by a more accurate information about the *local* speed of wave propagation. We start by assuming that in every cell, I_j , we have reconstructed a piecewise polynomial interpolant, $P_j(x, t^n)$, from the previously computed cell averages, $\{\bar{u}_j^n\}$. Then, an upper bound on the speed of propagation of discontinuities at the cell boundaries, $x_{j+1/2}$, is given by

$$a_{j+1/2}^n = \max_{u \in \mathcal{C}(u_{j+1/2}^-, u_{j+1/2}^+)} \rho\left(\frac{\partial f}{\partial u}(u)\right), \quad (3.1)$$

where $\rho(A)$ denotes the spectral radius of a matrix A , i.e., $\rho(A) := \max_i |\lambda_i(A)|$, with $\lambda_i(A)$ being its eigenvalues. We denote by $u_{j+1/2}^+$ and $u_{j+1/2}^-$ the left and right intermediate values of $u(x, t^n)$ at $x_{j+1/2}$, i.e.,

$$u_{j+1/2}^+ := P_{j+1}(x_{j+1/2}, t^n), \quad u_{j+1/2}^- := P_j(x_{j+1/2}, t^n),$$

and by $\mathcal{C}(u_{j+1/2}^-, u_{j+1/2}^+)$ a curve in phase space that connects $u_{j+1/2}^-$ and $u_{j+1/2}^+$ via the Riemann fan.

Remark: In most practical applications, these local maximal speeds can be easily evaluated. For example, in the genuinely nonlinear or linearly degenerate case one finds that (3.1) reduces to

$$a_{j+1/2}^n := \max \left\{ \rho\left(\frac{\partial f}{\partial u}(u_{j+1/2}^-)\right), \rho\left(\frac{\partial f}{\partial u}(u_{j+1/2}^+)\right) \right\}. \quad (3.2)$$

Given the piecewise polynomial interpolant at time t^n , $\{P_j(x, t^n)\}$, and the local speeds of propagation, $\{a_{j+1/2}^n\}$, we construct the fully-discrete, central method in two steps, which are schematically described in Figure 3.1. First, we integrate over the control volumes, $[x_{j-1/2,l}^n, x_{j-1/2,r}^n] \times [t^n, t^{n+1}]$, $[x_{j-1/2,r}^n, x_{j+1/2,l}^n] \times [t^n, t^{n+1}]$, and $[x_{j+1/2,l}^n, x_{j+1/2,r}^n] \times [t^n, t^{n+1}]$, obtaining $\bar{w}_{j-1/2}^{n+1}$, \bar{w}_j^{n+1} and $\bar{w}_{j+1/2}^{n+1}$, respectively. Due to the finite speed of propagation, the points $x_{j+1/2,l}^n$ and $x_{j+1/2,r}^n$,

$$x_{j+1/2,l}^n := x_{j+1/2} - a_{j+1/2}^n \Delta t, \quad x_{j+1/2,r}^n := x_{j+1/2} + a_{j+1/2}^n \Delta t,$$

separate between smooth and non-smooth regions. That is, the solution of equation (1.1) subject to the piecewise polynomial initial data prescribed at time $t = t^n$, may be non-smooth only inside the intervals $[x_{j+1/2,l}^n, x_{j+1/2,r}^n]$ for $t \in [t^n, t^{n+1}]$.

In the second step, we repeat the non-oscillatory reconstruction (this time on a nonuniformly spaced grid) and project the obtained reconstruction on the original, uniform grid, ending up with the cell averages at the next time level t^{n+1} , $\{\bar{u}_j^{n+1}\}$. This last step does not involve time integration, and was introduced in the context of changing staggered methods into non-staggered methods in [10].

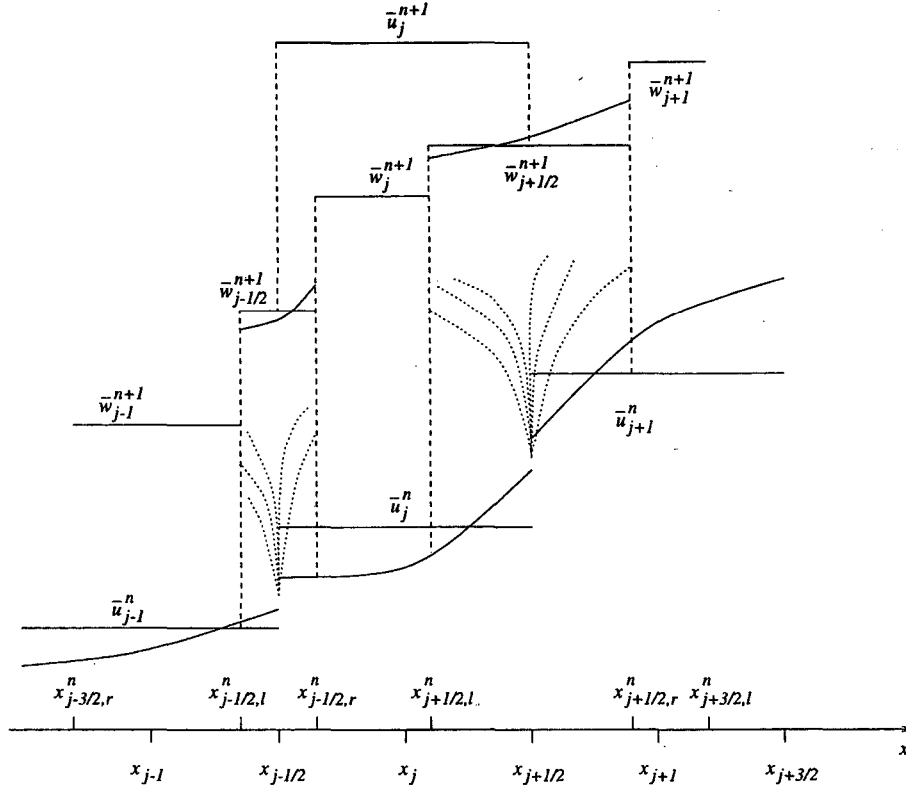


Figure 3.1: Modified Central Differencing

We now turn to the detailed description of this algorithm. Assume that the piecewise polynomial reconstruction in cell I_j at time t^n is of the form

$$P_j(x, t^n) = A_j + B_j(x - x_j) + \frac{1}{2}C_j(x - x_j)^2. \quad (3.3)$$

Then a direct computation of the integrals over the control volumes, $[x_{j+1/2,l}^n, x_{j+1/2,r}^n] \times [t^n, t^{n+1}]$ and $[x_{j-1/2,r}^n, x_{j+1/2,l}^n] \times [t^n, t^{n+1}]$, yields

$$\begin{aligned} \bar{w}_{j+1/2}^{n+1} = & \frac{A_j + A_{j+1}}{2} + \frac{\Delta x - a_{j+1/2}^n \Delta t}{4} (B_j - B_{j+1}) + \\ & + \left(\frac{\Delta x^2}{16} - \frac{a_{j+1/2}^n \Delta t \Delta x}{8} + \frac{(a_{j+1/2}^n \Delta t)^2}{12} \right) (C_j + C_{j+1}) - \\ & - \frac{1}{2a_{j+1/2}^n \Delta t} \left\{ \int_{t^n}^{t^{n+1}} [f(u(x_{j+1/2,r}^n, t)) dt - f(u(x_{j+1/2,l}^n, t))] dt \right\}; \end{aligned} \quad (3.4)$$

and

$$\begin{aligned} \bar{w}_j^{n+1} = & A_j + \frac{\Delta t}{2} (a_{j-1/2}^n - a_{j+1/2}^n) B_j + \\ & + \left[\frac{(\Delta x)^2}{24} - \frac{\Delta t \Delta x}{12} (a_{j-1/2}^n + a_{j+1/2}^n) + \frac{(\Delta t)^2}{6} \left((a_{j-1/2}^n)^2 - a_{j-1/2}^n a_{j+1/2}^n + (a_{j+1/2}^n)^2 \right) \right] C_j - \end{aligned} \quad (3.5)$$

$$-\frac{1}{\Delta x - \Delta t(a_{j-1/2}^n - a_{j+1/2}^n)} \left\{ \int_{t^n}^{t^{n+1}} [f(u(x_{j+1/2,l}^n, t))dt - f(u(x_{j-1/2,r}^n, t))] dt \right\},$$

respectively. To complete these computations, one should approximate the flux integrals on the RHS of (3.4) and (3.5) using, e.g., Simpson's quadrature as described in §2.

At this stage, the approximate cell averages, $\{\bar{w}_{j+\frac{1}{2}}^{n+1}, \bar{w}_j^{n+1}\}$, realize the solution at $t = t^{n+1}$ over a nonuniform grid, which is oversampled by twice the number of the original cells at $t = t^n$. To convert these nonuniform averages back into the original grid, we proceed along the lines of [10].

First, from the cell averages, $\bar{w}_{j+\frac{1}{2}}^{n+1}, \bar{w}_j^{n+1}$, given by (3.4)–(3.5), we reconstruct a third-order, piecewise polynomial, non-oscillatory interpolant (e.g., the CWENO interpolant described in §2.1), which we will denote by $\tilde{w}_{j+1/2}^{n+1}(x)$ and $\tilde{w}_j^{n+1}(x)$, respectively. In fact, we do not need any high-order reconstruction $\tilde{w}_j^{n+1}(x)$ since it will be averaged out (consult Figure 3.1).

We note in passing that even for a nonuniform grid data, the CWENO interpolant can be written explicitly (in the spirit of §2.1), but these details are irrelevant for the semi-discrete scheme, which will be described in §4. At that point, all that we need is to assume that such a reconstruction exists and that for all j it takes the form

$$\begin{aligned} \tilde{w}_{j+1/2}^{n+1}(x) &= \tilde{A}_{j+1/2} + \tilde{B}_{j+1/2}(x - x_{j+1/2}) + \frac{1}{2}\tilde{C}_{j+1/2}(x - x_{j+1/2})^2, \\ \tilde{w}_j^{n+1}(x) &= \bar{w}_j^{n+1}, \end{aligned} \quad (3.6)$$

in the non-smooth region, $(x_{j+1/2,l}^n, x_{j+1/2,r}^n)$, and in the smooth region, $(x_{j-1/2,r}^n, x_{j+1/2,l}^n)$, respectively. Given (3.4), (3.5) and (3.6), we conclude by computing the new cell averages at time t^{n+1} according to

$$\begin{aligned} \bar{w}_j^{n+1} &= \frac{1}{\Delta x} \left[\int_{x_{j-1/2}}^{x_{j-1/2,r}^n} \tilde{w}_{j-1/2}^{n+1}(x)dx + \int_{x_{j-1/2,r}^n}^{x_{j+1/2,l}^n} \tilde{w}_j^{n+1}(x)dx + \int_{x_{j+1/2,l}^n}^{x_{j+1/2}} \tilde{w}_{j+1/2}^{n+1}(x)dx \right] = \\ &= \lambda a_{j-1/2}^n \tilde{A}_{j-1/2} + [1 - \lambda(a_{j-1/2}^n + a_{j+1/2}^n)] \bar{w}_j^{n+1} + \lambda a_{j+1/2}^n \tilde{A}_{j+1/2} + \\ &\quad + \frac{\lambda \Delta t}{2} \left((a_{j-1/2}^n)^2 \tilde{B}_{j-1/2} - (a_{j+1/2}^n)^2 \tilde{B}_{j+1/2} \right) + \\ &\quad + \frac{\lambda (\Delta t)^2}{6} \left((a_{j-1/2}^n)^3 \tilde{C}_{j-1/2} + (a_{j+1/2}^n)^3 \tilde{C}_{j+1/2} \right). \end{aligned} \quad (3.7)$$

Remark: The third-order reconstruction (3.6) is necessary in order to guarantee the overall third-order accuracy, since simple averaging over $[x_{j-\frac{1}{2}}, x_{j+\frac{1}{2}}]$ (without reconstruction) reduces the order of the resulting scheme (see [10]).

4 The Semi-Discrete Scheme

We are now ready to derive our main result, which is the new third-order, semi-discrete, central scheme. First, we describe our ideas in the one-dimensional framework and then we

extend them to multidimensional problems.

4.1 One-Dimensional Problems

We start with the derivation of the third-order semi-discrete scheme for one-dimensional (systems of) hyperbolic conservation laws. Using the fully-discrete scheme obtained in §3, the semi-discrete approximation can be directly written as the limit

$$\frac{d}{dt}\bar{u}_j(t) = \lim_{\Delta t \rightarrow 0} \frac{\bar{u}_j^{n+1} - \bar{u}_j^n}{\Delta t}. \quad (4.1)$$

Substituting (3.7) into (4.1) results with

$$\begin{aligned} \frac{d\bar{u}_j}{dt} = \lim_{\Delta t \rightarrow 0} \left\{ \frac{1}{\Delta x} a_{j-1/2}^n \tilde{A}_{j-1/2} - \frac{1}{\Delta x} (a_{j-1/2}^n + a_{j+1/2}^n) \bar{w}_j^{n+1} + \frac{1}{\Delta x} a_{j+1/2}^n \tilde{A}_{j+1/2} + \right. \\ \left. + \frac{1}{\Delta t} (\bar{w}_j^{n+1} - \bar{u}_j^n) \right\}. \end{aligned} \quad (4.2)$$

In the limit as $\Delta t \rightarrow 0$, all the Riemann fans have zero widths and therefore,

$$\tilde{A}_{j+1/2} = \bar{w}_{j+1/2}^{n+1}, \quad \tilde{A}_{j-1/2} = \bar{w}_{j-1/2}^{n+1}. \quad (4.3)$$

Using (3.3) we can also obtain

$$\begin{aligned} u(x_{j+1/2,r}^n, t) &\longrightarrow P_{j+1}(x_{j+1/2}, t) = A_{j+1} - \frac{\Delta x}{2} B_{j+1} + \frac{(\Delta x)^2}{8} C_{j+1} =: u_{j+1/2}^+(t), \\ u(x_{j+1/2,l}^n, t) &\longrightarrow P_j(x_{j+1/2}, t) = A_j + \frac{\Delta x}{2} B_j + \frac{(\Delta x)^2}{8} C_j =: u_{j+1/2}^-(t). \end{aligned}$$

Finally, plugging (3.4), (3.5) and (4.3) into (4.2) we compute the time limit explicitly, ending up with our new semi-discrete scheme,

$$\begin{aligned} \frac{d\bar{u}_j}{dt} = -\frac{1}{2\Delta x} \left[f(u_{j+1/2}^+(t)) + f(u_{j+1/2}^-(t)) - f(u_{j-1/2}^+(t)) - f(u_{j-1/2}^-(t)) \right] + \\ + \frac{a_{j+1/2}(t)}{2\Delta x} \left[u_{j+1/2}^+(t) - u_{j+1/2}^-(t) \right] - \frac{a_{j-1/2}(t)}{2\Delta x} \left[u_{j-1/2}^+(t) - u_{j-1/2}^-(t) \right], \end{aligned} \quad (4.4)$$

with local speeds $a_{j+1/2}(t)$, e.g., $a_{j+1/2}(t) := \max \left\{ \rho \left(\frac{\partial f}{\partial u} (u_{j+1/2}^-(t)) \right), \rho \left(\frac{\partial f}{\partial u} (u_{j+1/2}^+(t)) \right) \right\}$.

Remarks:

1. Our third-order scheme, (4.4), admits the conservative form,

$$\frac{d\bar{u}_j}{dt} = -\frac{H_{j+1/2}(t) - H_{j-1/2}(t)}{\Delta x}, \quad (4.5)$$

with the numerical flux

$$H_{j+1/2}(t) := \frac{f(u_{j+1/2}^+(t)) + f(u_{j+1/2}^-(t))}{2} - \frac{a_{j+1/2}(t)}{2} \left[u_{j+1/2}^+(t) - u_{j+1/2}^-(t) \right]. \quad (4.6)$$

This scheme is a natural generalization of the second-order semi-discrete scheme from [16]. Moreover, the second-order scheme has exactly the same form, (4.5)–(4.6); the only difference is in the more accurate computation of the intermediate values, $u_{j+1/2}^+(t)$ and $u_{j+1/2}^-(t)$. It is interesting to note that also the fully-discrete, staggered, second- and third-order central schemes have the same structure (see [27]).

2. Similar to the case of the second-order scheme, [16], the non-oscillatory property of the piecewise parabolic reconstruction, (3.3), will guarantee the non-oscillatory nature of our semi-discrete scheme. But unlike the piecewise linear reconstruction utilized in the second-order method, a piecewise parabolic reconstruction can be only essentially non-oscillatory. This means that, in principle, such a reconstruction may increase the total variation of the computed piecewise constant solution. Our numerical examples, however, demonstrate that the growth of the total variation is always bounded. Such desirable behavior of bounded total variation in the context of central-WENO schemes, was already observed in [23].
3. We would like to stress once again the simplicity of our new method, which does not require any (approximate) Riemann solver or any use of the characteristic variables – the reconstruction of piecewise polynomial interpolant, (3.3), is carried out *component-wise*. In particular, unlike the standard central schemes, but similar to the second-order semi-discrete method in [16], our method is based on one grid (and not on staggering between two grids). This can be a big advantage (compared with the traditional central schemes) when dealing with boundary conditions and complex geometries.

Next, let us consider the general convection-diffusion equation, (1.2). Similar to the case of the second-order semi-discrete scheme, [16], operator splitting is not needed. We can apply our third-order semi-discrete scheme, (4.5)–(4.6), to the (degenerate) parabolic equation, (1.2), in a straightforward manner. This results in the following scheme,

$$\frac{d\bar{u}_j}{dt} = -\frac{H_{j+1/2}(t) - H_{j-1/2}(t)}{\Delta x} + Q_j(t). \quad (4.7)$$

Here, $H_{j+1/2}(t)$ is our numerical convection flux, (4.6), and $Q_j(t)$ is a high-order approximation to the diffusion term, $Q(u, u_x)_x$. In the examples below we use the fourth-order central differencing of the form

$$Q_j(t) = \frac{1}{12\Delta x} \left[-Q(u_{j+2}(t), (u_x)_{j+2,j}) + 8Q(u_{j+1}(t), (u_x)_{j+1,j}) - 8Q(u_{j-1}(t), (u_x)_{j-1,j}) + Q(u_{j-2}(t), (u_x)_{j-2,j}) \right], \quad (4.8)$$

where

$$\begin{aligned} (u_x)_{j+2,j} &:= \frac{1}{12\Delta x} \left[25u_{j+2}(t) - 48u_{j+1}(t) + 36u_j - 16u_{j-1}(t) + 3u_{j-2}(t) \right], \\ (u_x)_{j+1,j} &:= \frac{1}{12\Delta x} \left[3u_{j+2}(t) + 10u_{j+1}(t) - 18u_j + 6u_{j-1}(t) - u_{j-2}(t) \right], \\ (u_x)_{j-1,j} &:= \frac{1}{12\Delta x} \left[u_{j+2}(t) - 6u_{j+1}(t) + 18u_j - 10u_{j-1}(t) - 3u_{j-2}(t) \right], \\ (u_x)_{j-2,j} &:= \frac{1}{12\Delta x} \left[-3u_{j+2}(t) + 16u_{j+1}(t) - 36u_j + 48u_{j-1}(t) - 25u_{j-2}(t) \right]; \end{aligned} \quad (4.9)$$

and $\{u_j(t)\}$ are point-values of the reconstructed polynomials, (3.3), i.e., $u_j(t) = P_j(x_j, t)$.

4.2 Multi-Dimensional Extensions

Without loss of generality, let us consider the *two-dimensional* (system of) convection-diffusion equations,

$$u_t + f(u)_x + g(u)_y = Q^x(u, u_x, u_y)_x + Q^y(u, u_x, u_y)_y, \quad (4.10)$$

where the case $Q^x \equiv Q^y \equiv 0$ corresponds to the 2D pure hyperbolic problem.

Suppose that we have computed an approximate solution to (4.10) at some time t , and have reconstructed a two-dimensional piecewise polynomial, third-order, essentially non-oscillatory interpolant over the uniform spatial grid, $(x_j, y_k) = (j\Delta x, k\Delta y)$.

Following [16], the 2D extension of our third-order semi-discrete scheme, (4.7),(4.6), can be written in the following form,

$$\begin{aligned} \frac{d\bar{u}_{j,k}}{dt} = & -\frac{H_{j+1/2,k}^x(t) - H_{j-1/2,k}^x(t)}{\Delta x} - \frac{H_{j,k+1/2}^y(t) - H_{j,k-1/2}^y(t)}{\Delta y} + \\ & + Q_{j,k}^x(t) + Q_{j,k}^y(t). \end{aligned} \quad (4.11)$$

Here, $H_{j+1/2,k}^x(t)$ and $H_{j,k+1/2}^y(t)$ are x - and y -numerical convection fluxes, respectively (they can be viewed as a generalization of the one-dimensional flux, (4.6)),

$$\begin{aligned} H_{j+1/2,k}^x(t) := & \frac{f(u_{j+1/2,k}^+(t)) + f(u_{j+1/2,k}^-(t))}{2} - \\ & - \frac{a_{j+1/2,k}^x(t)}{2} \left[u_{j+1/2,k}^+(t) - u_{j+1/2,k}^-(t) \right], \end{aligned} \quad (4.12)$$

$$\begin{aligned} H_{j,k+1/2}^y(t) := & \frac{g(u_{j,k+1/2}^+(t)) + g(u_{j,k+1/2}^-(t))}{2} - \\ & - \frac{a_{j,k+1/2}^y(t)}{2} \left[u_{j,k+1/2}^+(t) - u_{j,k+1/2}^-(t) \right]. \end{aligned}$$

The numerical fluxes, (4.12), are expressed in terms of the intermediate values, $u_{j+1/2,k}^\pm(t)$, $u_{j,k+1/2}^\pm(t)$, which are obtained from the piecewise polynomial reconstruction. The local speeds, $a_{j+1/2,k}^x(t)$ and $a_{j,k+1/2}^y(t)$, are computed, e.g., by

$$a_{j+1/2,k}^x(t) := \max \left\{ \rho \left(\frac{\partial f}{\partial u}(u_{j+1/2,k}^-(t)) \right), \rho \left(\frac{\partial f}{\partial u}(u_{j+1/2,k}^+(t)) \right) \right\}, \quad (4.13)$$

$$a_{j,k+1/2}^y(t) := \max \left\{ \rho \left(\frac{\partial g}{\partial u}(u_{j,k+1/2}^-(t)) \right), \rho \left(\frac{\partial g}{\partial u}(u_{j,k+1/2}^+(t)) \right) \right\}.$$

Finally, $Q_{j,k}^x(t)$ and $Q_{j,k}^y(t)$ are high-order, central differencing approximations to the diffusion terms, $Q^x(u, u_x, u_y)_x$ and $Q^y(u, u_x, u_y)_y$.

Remarks:

1. We would like to emphasize that the problem of constructing a two-dimensional, third-order, non-oscillatory interpolant is highly non-trivial. Several essentially 2D reconstructions were proposed in [20, 21, 22]. Alternatively, one can use one-dimensional CWENO reconstruction, direction by direction, in order to compute the intermediate values, $u_{j+1/2,k}^{\pm}(t)$ and $u_{j,k+1/2}^{\pm}(t)$.

Following is the recipe for the computation of $u_{j+1/2,k}^+$ (the computation of other intermediate values can be carried out in the similar way).

$$u_{j+1/2,k}^+ = w_L P_L^k(x_{j+1/2}) + w_R P_R^k(x_{j+1/2}) + w_C P_C^k(x_{j+1/2}), \quad (4.14)$$

where the P 's are the polynomials introduced in §2.1,

$$\begin{aligned} P_R^k(x) &= \bar{u}_{j,k} + \frac{\bar{u}_{j+1,k} - \bar{u}_{j,k}}{\Delta x}(x - x_j), & P_L^k(x) &= \bar{u}_{j,k} + \frac{\bar{u}_{j,k} - \bar{u}_{j-1,k}}{\Delta x}(x - x_j), \\ P_C^k(x) &= \bar{u}_{j,k} - \frac{1}{12}(\bar{u}_{j+1,k} - 2\bar{u}_{j,k} + \bar{u}_{j-1,k}) - \frac{1}{12}(\bar{u}_{j,k+1} - 2\bar{u}_{j,k} + \bar{u}_{j,k-1}) + \\ &+ \frac{\bar{u}_{j+1,k} - \bar{u}_{j-1,k}}{2\Delta x}(x - x_j) + \frac{\bar{u}_{j+1,k} - 2\bar{u}_{j,k} + \bar{u}_{j-1,k}}{\Delta x^2}(x - x_j)^2. \end{aligned} \quad (4.15)$$

The weights, w_L, w_R, w_C which are given by (2.9), and are based on the smoothness indicators in (2.10).

Note that the only difference between this reconstruction and the 1D reconstruction, (2.4)–(2.10), is an additional term in $P_C^k(x)$, $-\frac{1}{12}(\bar{u}_{j,k+1} - 2\bar{u}_{j,k} + \bar{u}_{j,k-1})$, which corresponds to the second derivative in the y direction and guarantees the third-order accuracy of the computed intermediate values.

This ‘dimension by dimension’ approach, was implemented in Example 5 below.

2. It is straightforward to extend the two-dimensional scheme, (4.11), to more space dimensions. In particular, the dimension-by-dimension approach is a very simple and promising approach for multi-dimensional problems.

5 Numerical Examples

We conclude the paper with a number of numerical examples. Here, in order to retain the overall high accuracy, the semi-discrete scheme is combined with a high-order, stable ODE solver to complete the spatio-temporal discretization. Numerically, we observed that a variety of explicit methods provide satisfactory results in the context of our semi-discrete scheme.

For the inviscid problems (Examples 1, 2, 3 and 5), we used the third-order total variation diminishing (TVD) Runge-Kutta type method introduced by Shu and Osher in [32]. However, if we apply this time-integration method or any other standard Runge-Kutta type method to (degenerate) parabolic problems, the time-step can be very small due to their strict stability restrictions.

To overcome this difficulty, we used (in Examples 4 and 5) the third-order ODE solver (called DUMKA3) by Medovikov, [28]. This explicit method has larger stability domains (compared with the standard Runge-Kutta methods), which allow larger time-steps. In practice, DUMKA3 works as fast as implicit methods (see [28] for details).

We abbreviate by SD3 our third-order semi-discrete scheme, which will be combined with the third-order TVD Runge-Kutta type method (RK3) or with DUMKA3.

Example 1: Linear Accuracy Test

Consider the scalar linear hyperbolic equation

$$u_t + u_x = 0, \quad x \in [0, 2\pi], \quad (5.1)$$

augmented with the smooth initial data, $u(x, 0) = \sin x$, and periodic boundary conditions. This simple problem admits a global classical solution, which was computed at time $T = 1$ with a varying number of grid points, N .

In Table 5.1 we check the accuracy of our third-order semi-discrete scheme, SD3, coupled with the RK3 ODE solver. If instead of computing the approximate convergence rate between two consecutive mesh refinings, one approximates the convergence rate between $N = 40$ and $N = 1280$, the results are 3.27 in the L^1 -norm and 2.91 in the L^∞ -norm. This clearly demonstrates that our scheme is third-order.

The error is measured in terms of the pointwise values,

$$\|\tilde{u} - u\|_{L^1} := \Delta x \sum_j |\tilde{u}_j(T) - u(x_j, T)|, \quad \|\tilde{u} - u\|_{L^\infty} := \max_j |\tilde{u}_j(T) - u(x_j, T)|.$$

Here, \tilde{u} is an approximate solution, which is realized by its values at the grid points, x_j ,

$$\tilde{u}_j(T) = P_j(x_j, T),$$

where the P_j 's are the piecewise parabolic interpolants, (3.3), constructed at the final time $t = T$.

N	L^1 -error	rate	L^∞ -error	rate
40	4.492e-02	-	2.822e-02	-
80	1.092e-02	2.04	1.065e-02	1.41
160	2.162e-03	2.34	3.426e-03	1.64
320	1.811e-04	3.58	4.705e-04	2.86
640	9.267e-06	4.29	2.267e-05	4.38
1280	5.409e-07	4.10	1.171e-06	4.27

Table 5.1: Accuracy test for the linear advection problem, (5.1); The errors at $T = 1$.

Example 2: Burgers' Equation

In this example we approximate solutions to the inviscid Burgers' equation,

$$u_t + \left(\frac{u^2}{2}\right)_x = 0, \quad x \in [0, 2\pi], \quad (5.2)$$

augmented with the smooth initial data, $u(x, 0) = 0.5 + \sin x$, and periodic boundary conditions.

The unique entropy solution of (5.2) develops a shock discontinuity at the critical time $T_c = 1$. Table 5.2 shows the L^1 - and L^∞ -norms of the errors at the pre-shock time $T = 0.5$, when the solution is still smooth. Once again, when approximating the convergence rate by looking at the errors for $N = 40$ and $N = 1280$, we get 3.25 in the L^1 -norm and 3.10 in the L^∞ -norm. These results indicate that our method is also third-order accurate when the accuracy is measured in nonlinear problems.

In Figures 5.1–5.2 we present the approximate solutions at the post-shock time $T = 2$, when the shock is well developed. The essentially non-oscillatory nature of our scheme can be clearly observed.

N	L^1 -error	rate	L^∞ -error	rate
40	2.370e-02	–	2.225e-02	–
80	5.759e-03	2.04	9.053e-03	1.30
160	1.161e-03	2.31	2.921e-03	1.63
320	9.541e-05	3.61	3.926e-04	2.90
640	4.882e-06	4.29	1.778e-05	4.46
1280	3.044e-07	4.00	5.732e-07	4.96

Table 5.2: Accuracy test for Burgers equation, (5.2); The pre-shock errors

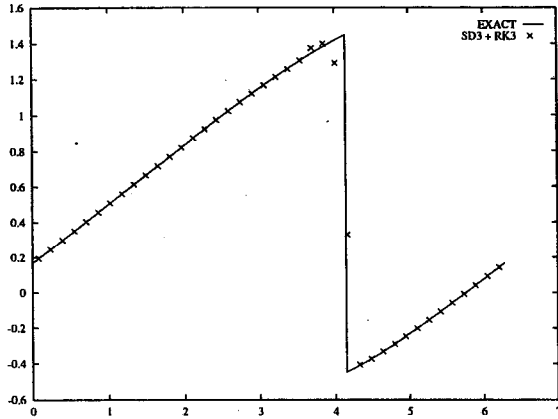


Figure 5.1: Burgers equation, (5.2); $T = 2$, $N=40$.

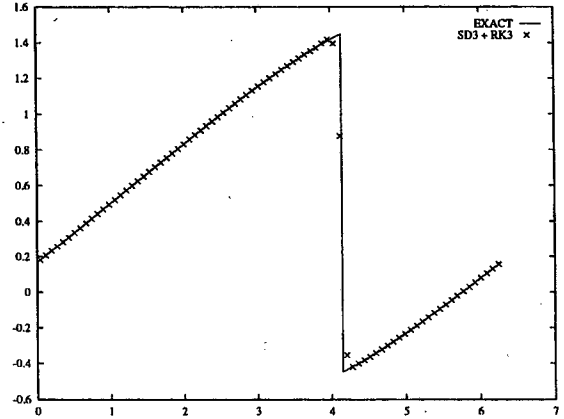


Figure 5.2: Burgers equation, (5.2); $T = 2$, $N=80$.

Example 3: Euler Equations of Gas Dynamics

Let us consider the one-dimensional Euler system,

$$\frac{\partial}{\partial t} \begin{bmatrix} \rho \\ m \\ E \end{bmatrix} + \frac{\partial}{\partial x} \begin{bmatrix} m \\ \rho u^2 + p \\ u(E + p) \end{bmatrix} = 0, \quad p = (\gamma - 1) \cdot \left(E - \frac{\rho}{2} u^2 \right),$$

where ρ , u , $m = \rho u$, p and E are the density, velocity, momentum, pressure and total energy, respectively. We solve this system subject to Sod's Riemann initial data, proposed in [33],

$$\vec{u}(x, 0) = \begin{cases} \vec{u}_L = (1, 0, 2.5)^T, & x < 0, \\ \vec{u}_R = (0.125, 0, 0.25)^T, & x > 0. \end{cases}$$

The approximations to the density, velocity and pressure obtained by the SD3 scheme with the RK3 time discretization are presented in Figures 5.3–5.8. The coefficient p in the smoothness indicator, (2.9)–(2.10), was taken as 0.6, which seems to be the optimal value in this specific example.

We would like to stress again that our SD3 scheme does not require the characteristic decomposition. To improve the resolution of the contact discontinuity, which is always smeared while the solution to the system of Euler equations is computed by the central method, we implemented the Artificial Compression Method (ACM) by Harten, [8]. In the context of central schemes, the ACM can be implemented as a corrector step to the component-wise approach (see [29] for details).

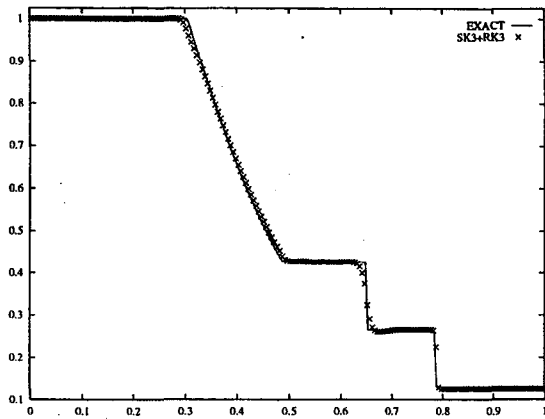


Figure 5.3: Sod problem - *density*.
 $N=200, T=0.1644$.

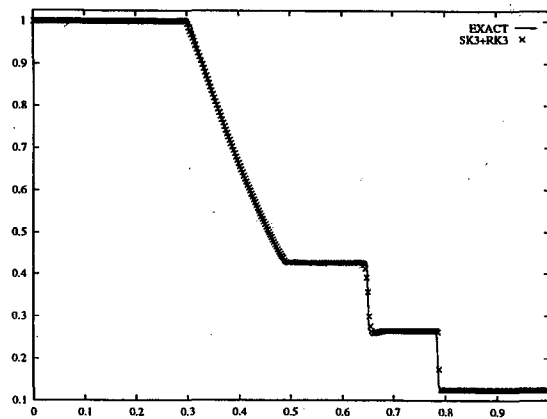


Figure 5.4: Sod problem - *density*.
 $N=400, T=0.1644$.

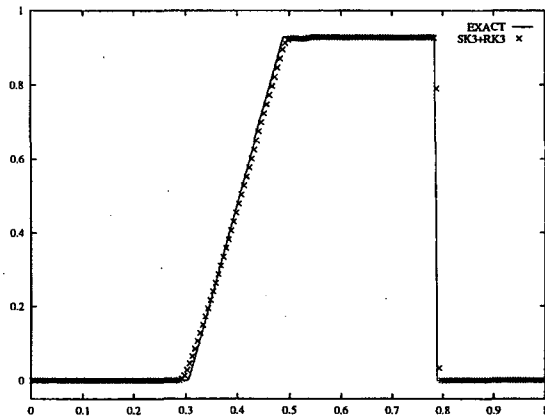


Figure 5.5: Sod problem - *velocity*.
 $N=200, T=0.1644$.

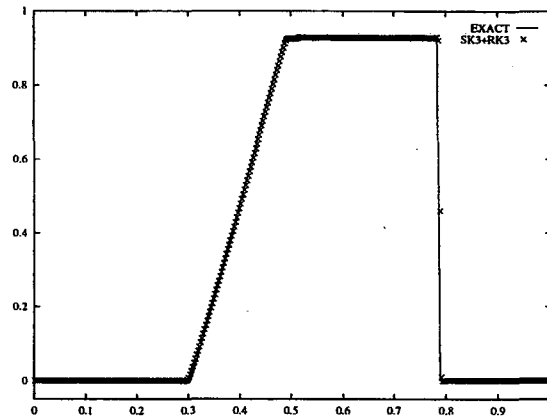


Figure 5.6: Sod problem - *velocity*.
 $N=400, T=0.1644$.

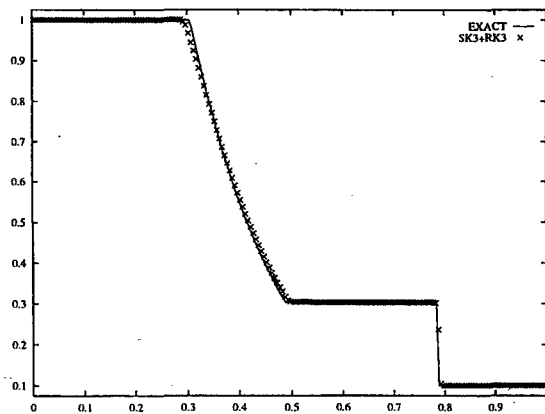


Figure 5.7: Sod problem - *pressure*.
 $N=200, T=0.1644$.

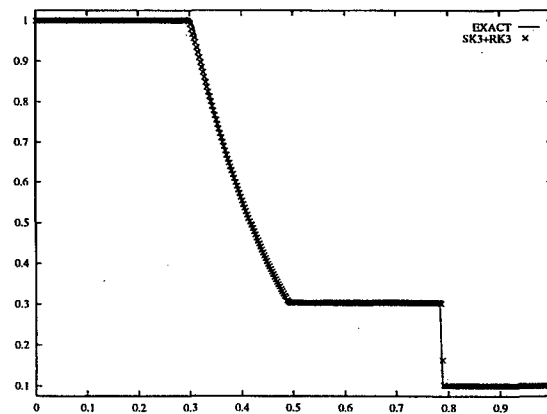


Figure 5.8: Sod problem - *pressure*.
 $N=400, T=0.1644$.

Example 4: Convection-Diffusion Equations – the Buckley-Leverett Model

In this example we solve the one-dimensional Buckley-Leverett equation,

$$u_t + f(u)_x = \varepsilon(\nu(u)u_x)_x, \quad \varepsilon\nu(u) \geq 0, \quad (5.3)$$

which can be viewed as a prototype model for the two-phase flow in oil reservoirs. Typically, $\nu(u)$ vanishes at some values of u , and thus (5.3) is a degenerate parabolic equation. Specifically, we take

$$f(u) = \frac{u^2}{u^2 + (1-u)^2}, \quad \nu(u) = 4u(1-u), \quad \varepsilon = 0.01,$$

and consider the initial value problem with the Riemann initial data,

$$u(x, 0) = \begin{cases} 0, & 0 \leq x < 1 - \frac{1}{\sqrt{2}}, \\ 1, & 1 - \frac{1}{\sqrt{2}} \leq x \leq 1. \end{cases} \quad (5.4)$$

The numerical solution to this problem, obtained by the SD3 scheme augmented with the DUMKA3 ODE solver, is presented in Figure 5.9.

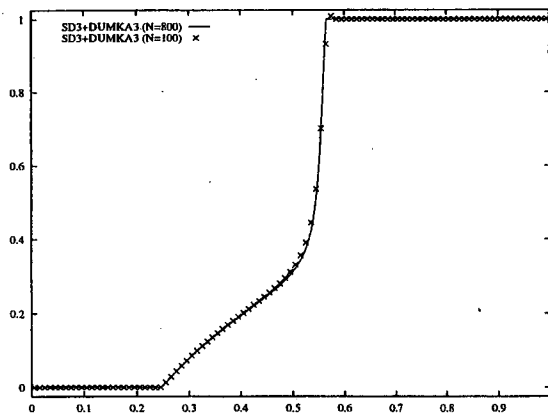


Figure 5.9: Buckley-Leverett model, (5.3)–(5.4). $\mathbf{T=0.2}$.

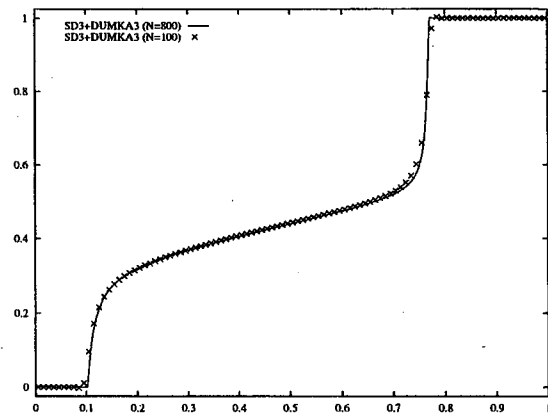


Figure 5.10: Buckley-Leverett model, (5.3)–(5.4), including the gravitational effect, (5.5). $\mathbf{T=0.2}$.

The model, (5.3), becomes more complicated by adding the effects of gravitation. This can be obtained, e.g., by taking

$$f(u) = \frac{u^2}{u^2 + (1-u)^2} (1 - 5(1-u)^2), \quad (5.5)$$

which is non-monotone on the interval $u \in [0, 1]$.

The numerical solution to this initial value problem is shown in Figure 5.10. Note that the exact solution to problem (5.3)–(5.4) is not available, but our solutions seem to converge to the physically relevant solutions in the both cases – with gravitation or without it.

Example 5: Incompressible Euler and Navier-Stokes equations

In this example we consider two-dimensional viscous and inviscid incompressible flow governed by the Navier-Stokes ($\nu > 0$) and by the Euler ($\nu = 0$) equations,

$$\vec{u}_t + (\vec{u} \cdot \nabla) \vec{u} + \nabla p = \nu \Delta \vec{u}. \quad (5.6)$$

Here, p denotes the pressure, and $\vec{u} = (u, v)$ is the two-component divergence-free velocity field, satisfying

$$u_x + v_y = 0. \quad (5.7)$$

In the 2D case (5.6) admits an equivalent scalar formulation in terms of the vorticity,

$$\omega_t + (u\omega)_x + (v\omega)_y = \nu \Delta \omega, \quad (5.8)$$

where $\omega := v_x - u_y$. The incompressibility, (5.7), implies that equation (5.8) can be written in an equivalent conservative form,

$$\omega_t + f(\omega)_x + g(\omega)_y = \nu \Delta \omega, \quad (5.9)$$

with a *global* convection flux, $(f, g) := (u\omega, v\omega)$. A second-order, fully-discrete, staggered, central scheme was used to solve the two-dimensional vorticity equations in [24]. This scheme was proved to satisfy a maximum principle for the vorticity. (For an equivalent scheme in the velocity formulation, see [13]).

When applied to equation (5.9), our two-dimensional, third-order, semi-discrete scheme, (4.11)–(4.13), takes the form,

$$\frac{d\bar{\omega}_{j,k}}{dt} = -\frac{H_{j+1/2,k}^x(t) - H_{j-1/2,k}^x(t)}{\Delta x} - \frac{H_{j,k+1/2}^y(t) - H_{j,k-1/2}^y(t)}{\Delta y} + \nu Q_{j,k}(t); \quad (5.10)$$

with the numerical convection fluxes,

$$\begin{aligned} H_{j+1/2,k}^x(t) &= \frac{u_{j+1/2,k}(t)}{2} \left[\omega_{j+1/2,k}^+(t) + \omega_{j+1/2,k}^-(t) \right] - \\ &\quad - \frac{a_{j+1/2,k}^x(t)}{2} \left[\omega_{j+1/2,k}^+(t) - \omega_{j+1/2,k}^-(t) \right], \end{aligned} \quad (5.11)$$

$$\begin{aligned} H_{j,k+1/2}^y(t) &= \frac{v_{j,k+1/2}(t)}{2} \left[\omega_{j,k+1/2}^+(t) + \omega_{j,k+1/2}^-(t) \right] - \\ &\quad - \frac{a_{j,k+1/2}^y(t)}{2} \left[\omega_{j,k+1/2}^+(t) - \omega_{j,k+1/2}^-(t) \right], \end{aligned}$$

and the local speeds,

$$a_{j+1/2,k}^x(t) := |u_{j+1/2,k}(t)|, \quad a_{j,k+1/2}^y(t) := |v_{j,k+1/2}(t)|. \quad (5.12)$$

To approximate the linear viscosity, $\Delta \omega$, we used the fourth-order central differencing,

$$\begin{aligned} Q_{j,k}(t) &= \frac{-\omega_{j+2,k}(t) + 16\omega_{j+1,k}(t) - 30\omega_{j,k}(t) + 16\omega_{j-1,k}(t) - \omega_{j-2,k}(t)}{12\Delta x^2} + \\ &\quad + \frac{-\omega_{j,k+2}(t) + 16\omega_{j,k+1}(t) - 30\omega_{j,k}(t) + 16\omega_{j,k-1}(t) - \omega_{j,k-2}(t)}{12\Delta y^2}. \end{aligned} \quad (5.13)$$

To compute the intermediate values of the vorticity, we use the ‘dimension by dimension’ approach described in §4.2: we reconstruct the corresponding CWENO interpolants in the x - and y -directions to obtain the values of $\omega_{j+1/2,k}^\pm$ and $\omega_{j,k+1/2}^\pm$.

Another important point in the incompressible computations is that in every time step one has to recover the velocities, $\{u_{j,k}, v_{j,k}\}$, from the known values of the vorticity, $\{\omega_{j,k}\}$. This can be done in many different ways (consult, e.g., [24] and the references therein). Here we have used a stream-function, ψ , such that $\Delta\psi = -\omega$, which is obtained by solving the nine-points Laplacian, $\Delta\psi_{j,k} = -\omega_{j,k}(t)$. This provides the values of the stream-function with fourth-order accuracy. Its gradient, $\nabla\psi$, then recovers the velocity field,

$$u_{j,k}(t) = \frac{-\psi_{j,k+2} + 8\psi_{j,k+1} - 8\psi_{j,k-1} + \psi_{j,k-2}}{12\Delta y},$$

$$v_{j,k}(t) = \frac{\psi_{j+2,k} - 8\psi_{j+1,k} + 8\psi_{j-1,k} - \psi_{j-2,k}}{12\Delta x}.$$
(5.14)

Remarks:

1. Observe that in this way we retain the discrete incompressibility, namely the discrete velocities computed in (5.14) satisfy

$$\frac{-u_{j+2,k} + 8u_{j+1,k} - 8u_{j-1,k} + u_{j-2,k}}{12\Delta x} + \frac{-v_{j,k+2} + 8v_{j,k+1} - 8v_{j,k-1} + v_{j,k-2}}{12\Delta y} = 0.$$

2. The point-values of the vorticity, which are required for using the nine-points Laplacian, were computed from its cell averages using the ‘dimension by dimension’ recipe, (4.14)–(4.15).

Finally, the intermediate values of velocities can be computed, e.g., using fourth-order averaging,

$$u_{j+1/2,k}(t) = \frac{-u_{j+2,k}(t) + 9u_{j+1,k}(t) + 9u_{j-1,k}(t) - u_{j-2,k}(t)}{16},$$

$$v_{j,k+1/2}(t) = \frac{-v_{j,k+2}(t) + 9v_{j,k+1}(t) + 9v_{j,k-1}(t) - v_{j,k-2}(t)}{16}.$$
(5.15)

We start our numerical experiments by checking the accuracy of our scheme, (5.10)–(5.15), augmented with the DUMKA3 time discretization. We consider the Navier-Stokes equations, (5.6)–(5.7) with $\nu = 0.05$, subject to the smooth periodic initial data (taken from [4]),

$$u(x, y, 0) = -\cos(x) \sin(y), \quad v(x, y, 0) = \sin(x) \cos(y),$$
(5.16)

The exact solution to this problem is simply an exponential decay of the initial data, given by

$$u(x, y, t) = -\cos(x) \sin(y) e^{-2\nu t}, \quad v(x, y, t) = \sin(x) \cos(y) e^{-2\nu t}.$$

$N_x \times N_y$	L^∞ -error	rate	L^1 -error	rate	L^2 -error	rate
32*32	2.429e-02	-	1.791e-01	-	4.559e-02	-
64*64	4.571e-03	2.41	2.814e-02	2.67	7.635e-03	2.58
128*128	8.342e-04	2.45	3.869e-03	2.86	1.146e-03	2.74
256*256	1.208e-04	2.79	4.966e-04	2.96	1.502e-04	2.93

Table 5.3: Accuracy Test for the Navier-Stokes Equations. (5.6)–(5.7), (5.16), $\nu = 0.05$. Errors at $T = 2$

The approximate solution with different number of grid points was computed at time $t = 2$. The errors, measured in terms of vorticity in the L^∞ -, L^1 - and L^2 -norms are shown in Table 5.3.

Next, the third-order semi-discrete scheme, (5.10)–(5.15), was implemented for the periodic double shear-layer model problem taken from [2]. First, we solve the Euler equations, (5.6)–(5.7) with $\nu = 0$, subject to the $(2\pi, 2\pi)$ -periodic initial data,

$$u(x, y, 0) = \begin{cases} \tanh(\frac{1}{\rho}(y - \pi/2)), & y \leq \pi, \\ \tanh(\frac{1}{\rho}(3\pi/2 - y)), & y > \pi, \end{cases} \quad v(x, y, 0) = \delta \cdot \sin(x). \quad (5.17)$$

Here, the "thick" shear-layer width parameter, ρ , is taken as $\frac{\pi}{15}$ and the perturbation parameter $\delta = 0.05$.

The numerical results at times $T = 4, 6, 10$ with $N = 64 \times 64$ and $N = 128 \times 128$ grid points are presented in Figures 5.11–5.16 and 5.19–5.20. In order to compare the quality of the results obtained with our new method, to previous results, we plot in Figures 5.17–5.18 the results obtained for the same double shear-layer problem with the second-order central scheme proposed in [24]. Compared with the second-order method, the new third-order method, can better resolve the large gradients. Since we are using only an essentially non-oscillatory reconstruction, some oscillations are created with the third-order method (and not with the "fully" non-oscillatory second-order method).

Finally, we solve the Navier-Stokes (N-S) equations, (5.6)–(5.7) with $\nu = 0.01$, augmented with the "thick" shear-layer periodic initial data, (5.17).

The numerical results at time $T = 10$ with $N = 64 \times 64$ and $N = 128 \times 128$ grid points are presented in Figures 5.21–5.24.

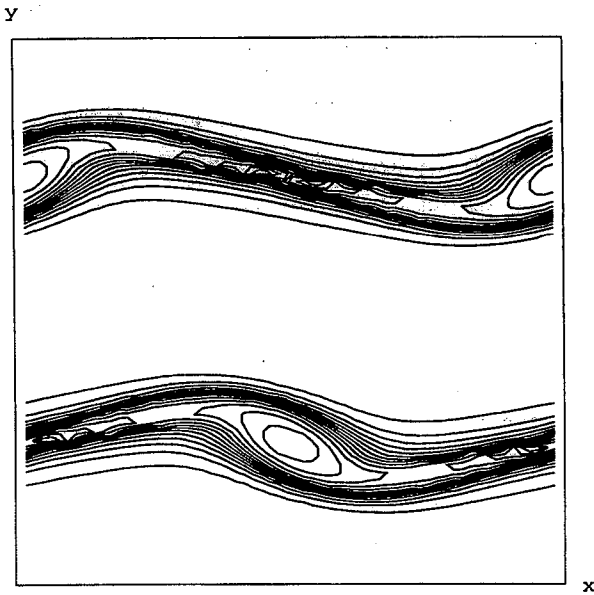


Figure 5.11: Incompressible Euler Equations; Third-order method; $T=4$, 64×64 grid.

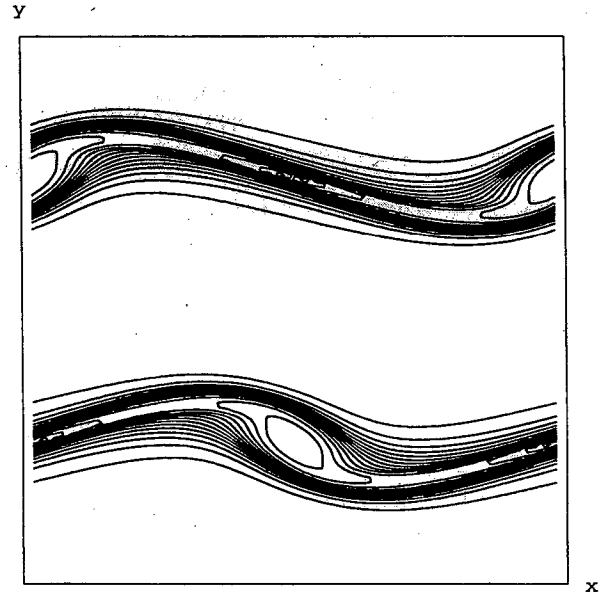


Figure 5.12: Incompressible Euler Equations; Third-order method; $T=4$, 128×128 grid.

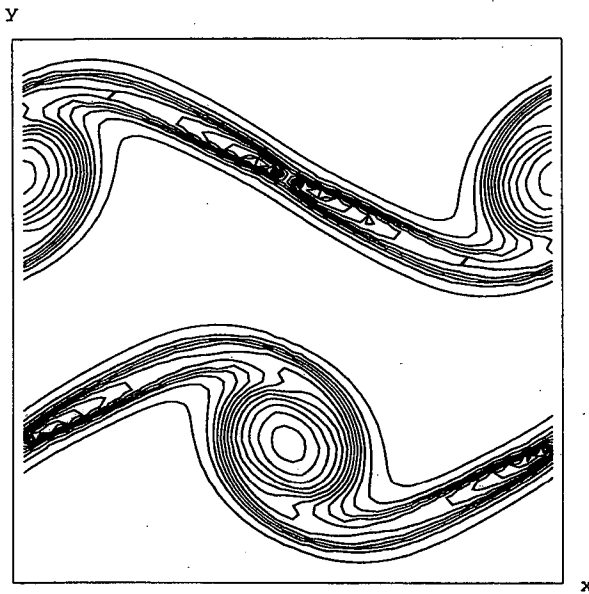


Figure 5.13: Incompressible Euler Equations; Third-order method; $T=6$, 64×64 grid.

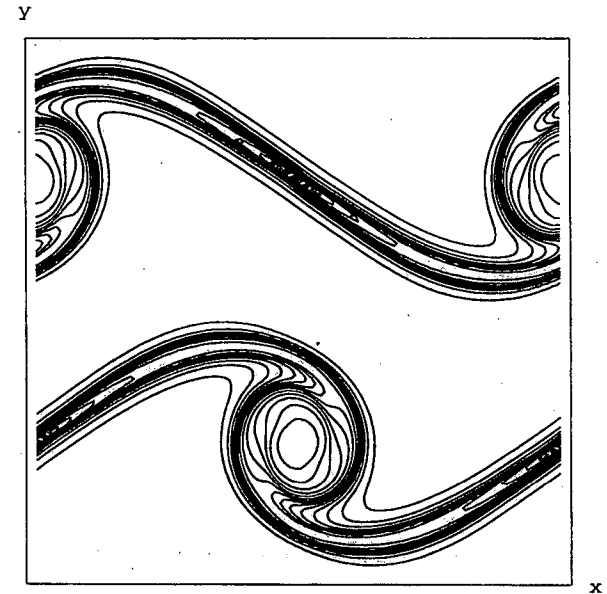


Figure 5.14: Incompressible Euler Equations; Third-order method; $T=6$, 128×128 grid.

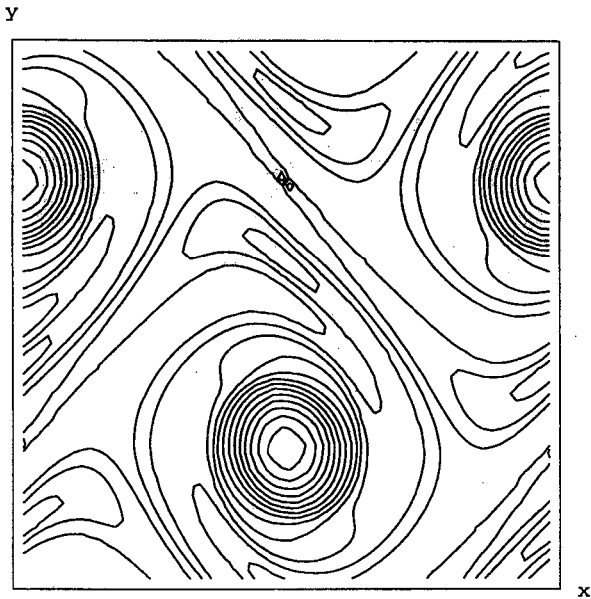


Figure 5.15: Incompressible Euler Equations; Third-order method; $T=10$, 64×64 grid.

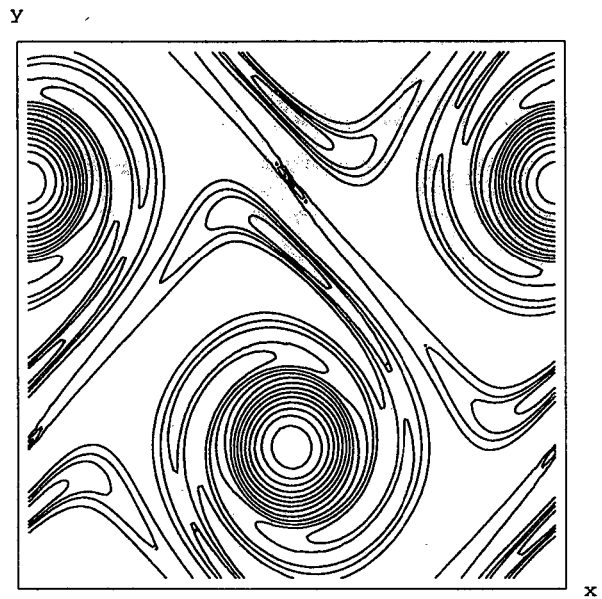


Figure 5.16: Incompressible Euler Equations; Third-order method; $T=10$, 128×128 grid.

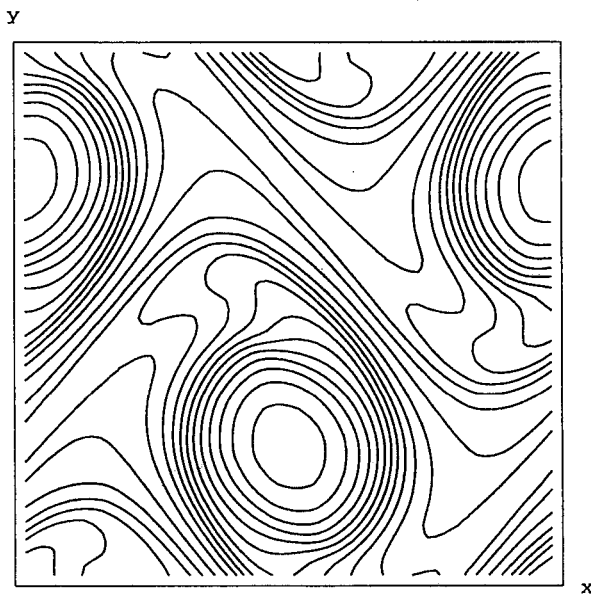


Figure 5.17: Incompressible Euler Equations; Second-order method; $T=10$, 64×64 grid.

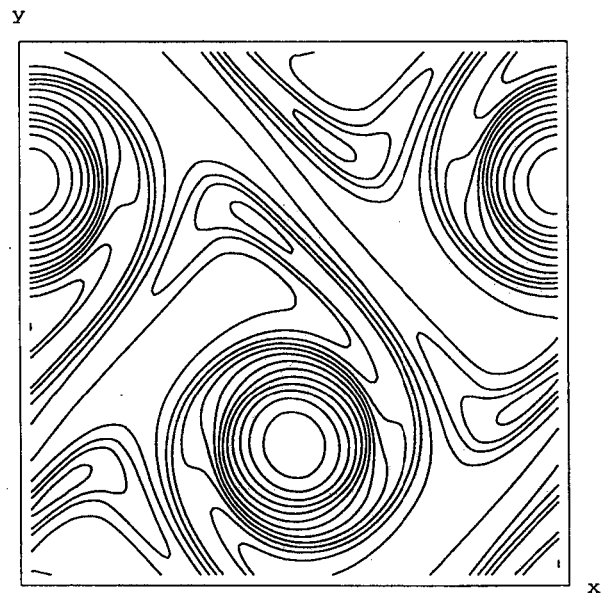


Figure 5.18: Incompressible Euler Equations; Second-order method; $T=10$, 128×128 grid.

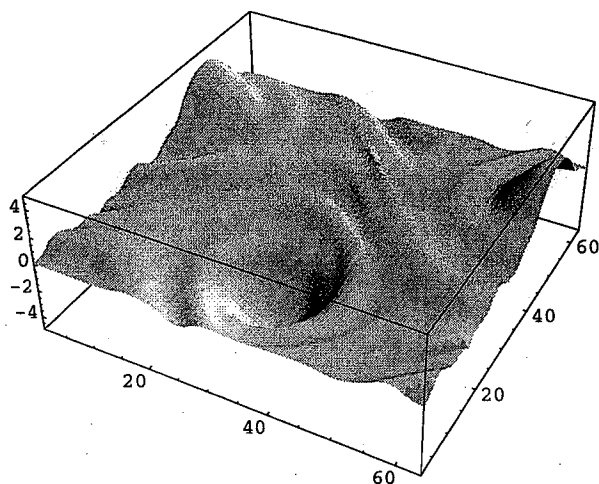


Figure 5.19: Incompressible Euler Equations; Third-order method; $T=10$, $64*64$ grid.

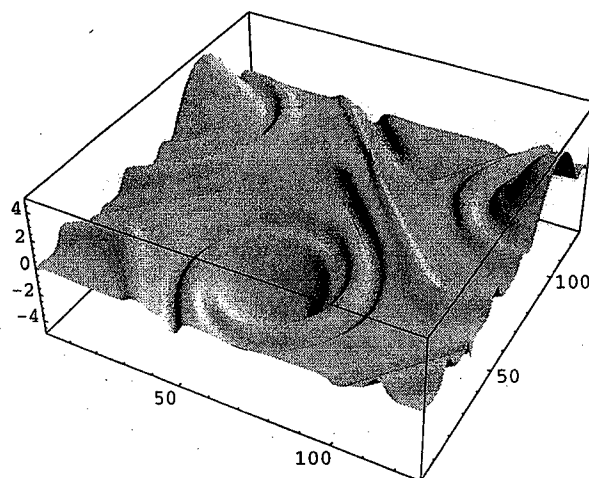


Figure 5.20: Incompressible Euler Equations; Third-order method; $T=10$, $128*128$ grid.

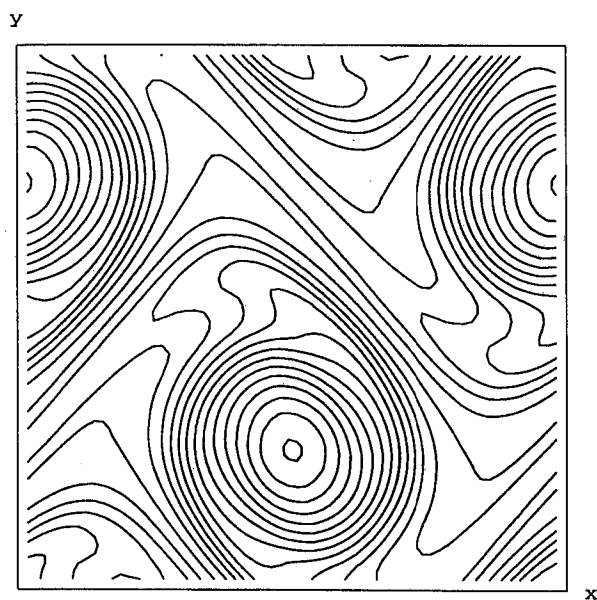


Figure 5.21: Incompressible Navier-Stokes Equations; Third-order method; $T=10$, $64*64$ grid.

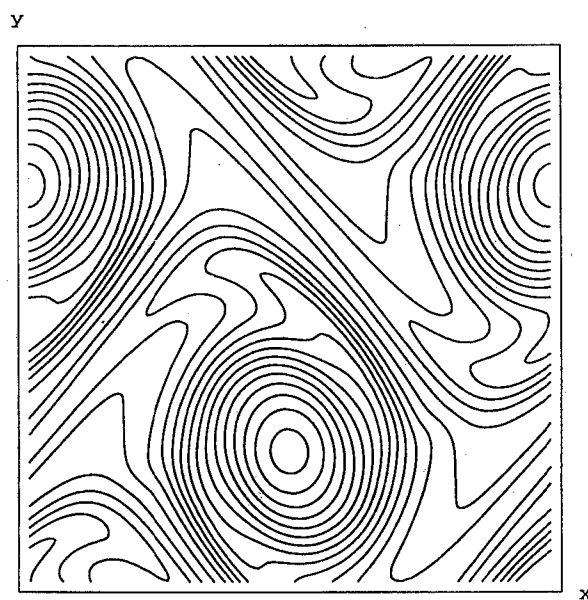


Figure 5.22: Incompressible Navier-Stokes Equations; Third-order method; $T=10$, $128*128$ grid.

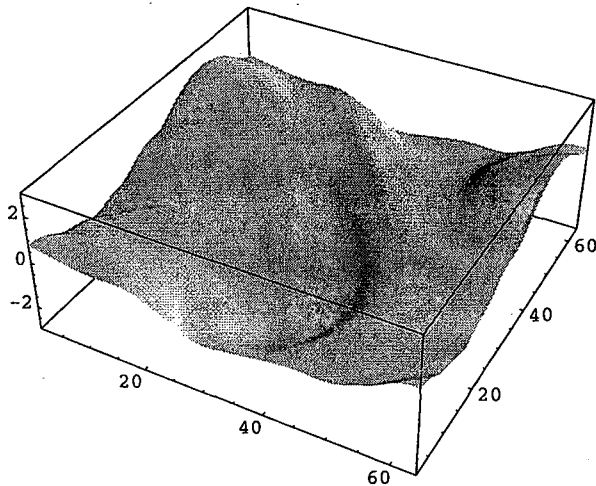


Figure 5.23: Incompressible Navier-Stokes Equations; Third-order method; $T=10$, $64*64$ grid.

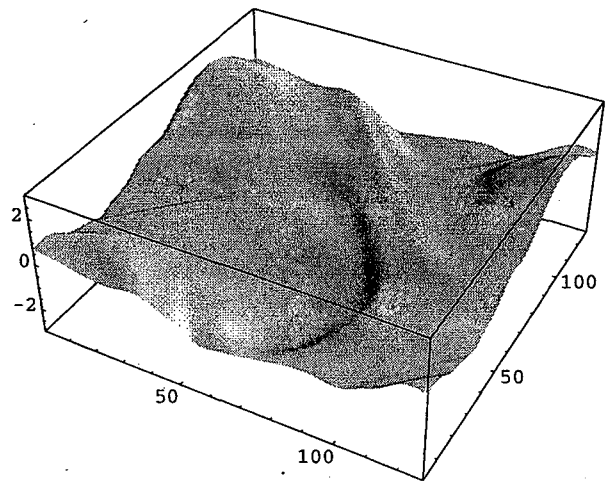


Figure 5.24: Incompressible Navier-Stokes Equations; Third-order method; $T=10$, $128*128$ grid.

Acknowledgment: The authors would like to thank Prof. S. Karni and Prof. R. Krasny for helpful comments. The work of A. Kurganov was supported in part by the NSF Group Infrastructure Grant. The work of D. Levy was supported in part by the Applied Mathematical Sciences subprogram of the Office of Science, U.S. Department of Energy, under contract DE-AC03-76-SF00098. Part of this work was done while A.K. was visiting the Lawrence Berkeley Lab.

References

- [1] Arminjon P., Viallon M.-C., *Généralisation du Schéma de Nessyahu-Tadmor pour Une Équation Hyperbolique à Deux Dimensions D'espace*, C.R. Acad. Sci. Paris, t. **320**, série I. (1995), pp.85–88.
- [2] Bell J. B., Colella P., Glaz H. M., *A Second-Order Projection Method for the Incompressible Navier-Stokes Equations*, JCP, **85**, (1989), pp.257–283.
- [3] Bianco F., Puppo G., Russo G., *High Order Central Schemes for Hyperbolic Systems of Conservation Laws*, SIAM J. Sci. Comp., to appear.
- [4] Chorin A., *Numerical Solution of the Navier-Stokes Equations*, Math. Comp., **22**, (1968), pp.745–762.
- [5] Friedrichs K. O., Lax P. D., *Systems of Conservation Equations with a Convex Extension*, Proc. Nat. Acad. Sci., **68**, (1971), pp.1686–1688.
- [6] Godlewski E., Raviart P.-A., *Numerical Approximation of Hyperbolic Systems of Conservation Laws*, Springer, New York, 1996.

- [7] Godunov S. K., *A Finite Difference Method for the Numerical Computation of Discontinuous Solutions of the Equations of Fluid Dynamics*, Mat. Sb., **47**, (1959), pp.271–290.
- [8] Harten A., *The Artificial Compression Method for Computation of Shocks and Contact Discontinuities, III. Self-Adjusting Hybrid Schemes*, Math. Comp., **32**, (1978), pp.363–389.
- [9] Harten A., Engquist B., Osher S., Chakravarthy S., *Uniformly High Order Accurate Essentially Non-oscillatory Schemes III*, JCP, **71**, (1987), pp.231–303.
- [10] Jiang G.-S., Levy D., Lin C.-T., Osher S., Tadmor E. *High-Resolution Non-Oscillatory Central Schemes with Non-Staggered Grids for Hyperbolic Conservation Laws*, SINUM, **35**, (1998), pp.2147–2168.
- [11] Jiang G.-S., Shu C.-W., *Efficient Implementation of Weighted ENO Schemes*, JCP, **126**, (1996), pp.202–228.
- [12] Jiang G.-S., Tadmor E., *Nonoscillatory Central Schemes for Multidimensional Hyperbolic Conservation Laws*, SIAM J. Sci. Comp., **19**, (1998), pp.1892–1917.
- [13] Kupferman R., Tadmor E., *A Fast High-Resolution Second-Order Central Scheme for Incompressible Flows*, Proc. Nat. Acad. Sci., **94**, (1997), pp. 4848–4852.
- [14] Kurganov A., Levy D., Rosenau P., *On Burgers-Type Equations with Nonmonotonic Dissipative Fluxes*, Comm. Pure Appl. Math., **51**, (1998), pp.443–473.
- [15] Kurganov A., Rosenau P., *Effects of a Saturating Dissipation in Burgers-Type Equations*, Comm. Pure Appl. Math., **50**, (1997), pp.753–771.
- [16] Kurganov A., Tadmor E., *New High-Resolution Central Schemes for Nonlinear Conservation Laws and Convection-Diffusion Equations*, submitted.
- [17] van Leer B., *Towards the ultimate conservative difference scheme, V. A second order sequel to Godunov's method*, JCP, **32**, (1979), pp. 101–136.
- [18] Levy D., *A Third-order 2D Central Schemes for Conservation Laws*, INRIA School on Hyperbolic Systems, Vol. I (1998), pp.489–504.
- [19] Levy D., Puppo G., Russo G., *Central WENO Schemes for Hyperbolic Systems of Conservation Laws*, M2AN, in press.
- [20] Levy D., Puppo G., Russo G., *A Third Order Central WENO Scheme for 2D Conservation Laws*, Appl. Nume. Math., in press.
- [21] Levy D., Puppo G., Russo G., *Compact Central WENO Schemes for Multidimensional Conservation Laws*, submitted.
- [22] Levy D., Puppo G., Russo G., *Central WENO Schemes for Multi-Dimensional Hyperbolic Systems of Conservation Laws*, in preparation.

- [23] Levy D., Puppo G., Russo G., *On the Behavior of the Total Variation in CWENO Methods for Conservation Laws*, Appl. Nume. Math., in press.
- [24] Levy D., Tadmor E., *Non-Oscillatory Central Schemes for the Incompressible 2-D Euler Equations*, Math. Res. Lett., **4**, (1997), pp.1-20.
- [25] Liu X.-D., Osher S., *Nonoscillatory High Order Accurate Self-Similar Maximum Principle Satisfying Shock Capturing Schemes I*, SINUM, **33**, no. 2 (1996), pp.760-779.
- [26] Liu X.-D., Osher S., Chan T., *Weighted Essentially Non-oscillatory Schemes*, JCP, **115**, (1994), pp.200-212.
- [27] Liu X.-D., Tadmor E., *Third Order Nonoscillatory Central Scheme for Hyperbolic Conservation Laws*, Numer. Math., **79**, (1998), pp.397-425.
- [28] Medovikov A.A., *High Order Explicit Methods for Parabolic Equations*, BIT, **38**, (1998) 2, pp.372-390.
- [29] Nessyahu H., Tadmor E., *Non-oscillatory Central Differencing for Hyperbolic Conservation Laws*, JCP, **87**, no. 2 (1990), pp.408-463.
- [30] Roe P. L., *Approximate Riemann Solvers, Parameter Vectors, and Difference Schemes*, JCP, **43**, (1981), pp.357-372.
- [31] Shu C.-W., *Numerical Experiments on the Accuracy of ENO and Modified ENO Schemes*, J. Sci. Comp., **5**, vol. 2, (1990), pp.127-149.
- [32] Shu C.-W., Osher S., *Efficient Implementation of Essentially Non-Oscillatory Shock-Capturing Schemes*, JCP, **77**, (1988), pp.439-471.
- [33] Sod G., *A Survey of Several Finite Difference Methods for Systems of Nonlinear Hyperbolic Conservation Laws*, JCP, **22**, (1978), pp.1-31.
- [34] Tadmor E., *Approximate Solutions of Nonlinear Conservation Laws*, CIME Lecture notes, 1997, UCLA CAM Report 97-51.

**ERNEST ORLANDO LAWRENCE BERKELEY NATIONAL LABORATORY
ONE CYCLOTRON ROAD | BERKELEY, CALIFORNIA 94720**